

Article

# Synthesis and Characterization of Spherical Calcium Carbonate Nanoparticles Derived from Cockle Shells

Abbas Ibrahim Hussein<sup>1,2</sup>, Zuryati Ab-Ghani<sup>1,3,\*</sup> , Ahmad Nazeer Che Mat<sup>4</sup>,  
Nur Atikah Ab Ghani<sup>4</sup>, Adam Husein<sup>1,3</sup> and Ismail Ab. Rahman<sup>4</sup>

<sup>1</sup> Prosthodontics Unit, School of Dental Sciences, Health Campus, Universiti Sains Malaysia, Kubang Kerian 16150, Kelantan, Malaysia; den.ani.abbas@uoanbar.edu.iq (A.I.H.); adamkck@usm.my (A.H.)

<sup>2</sup> Department of Prosthodontic Dentistry, College of Dentistry, University of Anbar, Ramadi 31001, Iraq

<sup>3</sup> Hospital Universiti Sains Malaysia, Kubang Kerian 16150, Kelantan, Malaysia

<sup>4</sup> Department of Biomaterials, School of Dental Sciences, Health Campus, Universiti Sains Malaysia, Kubang Kerian 16150, Kelantan, Malaysia; ahmadnazeerc@gmail.com (A.N.C.M.); nuratikahabdghani@gmail.com (N.A.A.G.); arismail@usm.my (I.A.R.)

\* Correspondence: zuryati@usm.my

Received: 12 September 2020; Accepted: 5 October 2020; Published: 14 October 2020



**Featured Application:** Spherical nano calcium carbonate will be used as a precursor to produce calcium oxide.

**Abstract:** Cockle shells are a natural reservoir of calcium carbonate ( $\text{CaCO}_3$ ), which is widely used in bone repair, tissue scaffolds, and the development of advanced drug delivery systems. Although many studies report on the preparation of  $\text{CaCO}_3$ , the development of a nanosized spherical  $\text{CaCO}_3$  precursor for calcium oxide ( $\text{CaO}$ ) that is suitable to be incorporated in dental material was scarce. Therefore, this study aimed to synthesize a nanosized spherical  $\text{CaCO}_3$  precursor for  $\text{CaO}$  derived from cockle shells using a sol–gel method. Cockle shells were crushed to powder form and mixed with hydrochloric acid, forming calcium chloride ( $\text{CaCl}_2$ ). Potassium carbonate ( $\text{K}_2\text{CO}_3$ ) was then fed to the diluted  $\text{CaCl}_2$  to obtain  $\text{CaCO}_3$ . The effect of experimental parameters on the morphology of  $\text{CaCO}_3$ , such as volume of water, type of solvents, feeding rate of  $\text{K}_2\text{CO}_3$ , and drying method, were investigated using field-emission scanning electron microscopy, energy-dispersive X-ray spectroscopy, X-ray diffractometry (XRD), Brunauer–Emmett–Teller surface area analysis, and thermogravimetric analysis. Optimized  $\text{CaCO}_3$  was then calcined to form  $\text{CaO}$ . XRD analysis of  $\text{CaCO}_3$  nanoparticles was indicative of the formation of a calcite phase. The well-structured spherical shape of  $\text{CaCO}_3$  was obtained by the optimum condition of the addition of 50 mL of water into  $\text{CaCl}_2$  in ethanolic solution with a 1 h feeding rate of  $\text{K}_2\text{CO}_3$ . Less agglomeration of  $\text{CaCO}_3$  was obtained using a freeze-drying technique with the surface area of  $26 \text{ m}^2/\text{g}$  and average particle size of 39 nm. Spherical shaped nanosized  $\text{CaO}$  (22–70 nm) was also synthesized. The reproducibility, low cost, and simplicity of the method suggest its potential applications in the large-scale synthesis of the nanoparticles, with spherical morphology in an industrial setting.

**Keywords:** calcium carbonate; calcium oxide; cockle shell; sol–gel method; morphological images; nanoparticles

## 1. Introduction

Calcium carbonate is an inorganic calcium salt which can be derived from shelled mollusks, limestone, coccolithophores, plant ashes, chalk, and marble [1,2]. It is considered to be a primary

source of CaO, which has been identified as a biological constituent of human bone. CaCO<sub>3</sub> is found abundantly in three natural polymorphs: calcite, vaterite, and aragonite. CaCO<sub>3</sub> nanoparticles with desired sizes, shapes, and morphologies has been extensively researched for their vast application in industrial, electronic, and agricultural fields [3].

Cockles are native to the coast of South East Asia (Thailand, Malaysia, and Indonesia) and are readily available as waste. Cockle shells are a natural reservoir of CaCO<sub>3</sub>, which is important for biomedical purposes [4]. In recent years, many reports have been documented on the application of CaCO<sub>3</sub> nanoparticles derived from cockle shells waste product, such as in drug delivery [5], polymer industries [6], biomedical scaffolds [7], and in nanomedicine [8]. The exploitation of solid waste such as the cockle shell makes the process more ecological, green, and cost-effective.

Nanoparticles are important for producing materials with good properties [9]. The small particle size provides a larger surface area for the particles to be uniformly dispersed, and therefore may enhance the mechanical properties of the material [10], hence making the material more resistant to degradation [11]. The physical and mechanical properties of these nanomaterials are dependent on their morphology [12]. Therefore, various methodologies have been devised to synthesize appropriate morphologies of these CaCO<sub>3</sub> nanoparticles. Spherical nanoparticles behave quite differently from layered silicates and fibers [13]. Their large surface area results in strong interfacial interactions between the filler and the polymer matrices in dental composite material [14], and provides them with their superior diffusion properties in various solvents [15]. Spherical nanoscale CaCO<sub>3</sub> fillers are most used in the preparation of nanocomposites and cementing materials for various uses [16]. The spherical particle structure is also important in producing a material with a higher glossiness and enamel-like reflection/refraction [17].

In dentistry, zirconia-based ceramics have been used as dental implants [18], and in crowns and bridges [19]. Pure zirconia has the disadvantage of cracking upon cooling, which can be avoided by adding a small percentage of oxide stabilizers like yttria (Y<sub>2</sub>O<sub>3</sub>), ceria (CeO<sub>2</sub>), magnesia (MgO), and calcia (CaO) [20–23]. Yttrium-stabilized zirconia is tough, with a fracture toughness of 5 to 10 MPa m<sup>1/2</sup> and a flexural strength of 900–1400 MPa [24,25], and it suffers from low-temperature aging degradation (LTAD) [26]. Although ceria-stabilized zirconia-alumina (Ce-TZP/A) can overcome the problem of LTAD, it is also among the toughest dental ceramic materials available, with a fracture toughness of 19 MPa m<sup>1/2</sup> and a flexural strength of 1400 MPa [24]. Both previously mentioned zirconia have the disadvantage of inferior machining associated with wear of the tool, due to their superior hardness. Therefore, other partially and fully stabilized zirconia, for example calcium oxide (CaO), may be used as replacement materials for dental application. A study has been conducted to produce calcia-doped zirconia for hip and knee replacement with modest fracture toughness (6 MPa m<sup>1/2</sup>) [27]. Therefore, calcia-stabilized zirconia is a possible material to give optimum strength, and at the same time it does not wear the milling machine. A study was also carried out to stabilize zirconia using CaO [28]. However, the particle size of stabilizers was not clearly specified. Furthermore, the shape of the CaO stabilizers produced was not spherical.

Currently, various template-aided methods such as Langmuir monolayers, functionalized polymer surfaces, and self-assembled monolayers are being used for the morphologically controlled synthesis of CaCO<sub>3</sub> nanoparticles [29]. However, these methods require expensive chemical decontamination, meticulous processing, sophisticated instrumentation, and a tedious and lengthy preparatory procedure, and therefore may not be suitable for large-scale synthesis.

The sol-gel synthetic method is among the most versatile technique, with advantages including the improvement of bonding with the chemical reaction taking place at low temperature, as well as simplicity and cost effectiveness [30]. Previous studies showed that factors such as temperature, solution pH, concentrations of reactants and surfactants, aging time, and nature of additives may influence the morphology, phases, and particle size of CaCO<sub>3</sub> crystals [31,32].

Even though many studies have been carried out to prepare CaCO<sub>3</sub> for various applications, to the best of the authors' knowledge, the development of spherical nano-CaO from a CaCO<sub>3</sub> precursor

derived from cockle shells using the sol–gel method has been scarcely reported. Furthermore, the shape and size of  $\text{CaCO}_3$  and  $\text{CaO}$  derived from cockle shell developed in previous studies were neither nanosized nor spherical [33–35]. The purpose of this study was to synthesize and characterize spherical nanoparticles of  $\text{CaCO}_3$  and  $\text{CaO}$  from cockle shells using the sol–gel method.

## 2. Materials and Methods

Cockle shells were obtained from a local beach, Pantai Bachok. The collected cockle shells were scrubbed under tap water with a brush to remove dirt and rinsed with double-distilled water (DDW). The cockle shells were finely crushed using a mortar and pestle, and then blended using a blender machine (Premier Super-g, India) into a fine cockle shell powder.

The powder was then sieved using a stainless-steel Sieve Shaker AS 200 Control (Retsch GmbH, Haan, Germany) with an aperture size of 63  $\mu\text{m}$  to obtain micron size (10–63  $\mu\text{m}$  diameter). Then, 5 g of micron-sized cockle shell powder was dissolved into 20 mL of 5 M hydrochloric acid (HCl) 37%, Emsure<sup>®</sup> (Merck KGaA, Darmstadt, Germany) to form calcium chloride ( $\text{CaCl}_2$ ). The solution was filtered with filter papers (Filters Fioroni Filter Circles 70 mm, Lab Logistic Group GmbH, Meckenheim, Germany). Contamination products were extracted from the solution using an electric mixer spun at 500 rpm for 1 h at room temperature. The formed  $\text{CaCl}_2$  was then diluted with 1 L DDW to form stock solution. Stock solution of  $\text{K}_2\text{CO}_3$  was prepared by dissolving 5 g of  $\text{K}_2\text{CO}_3$  ACS reagent,  $\geq 99\%$  (Sigma Aldrich, Steinheim, Germany) in 100 mL of DDW.

Different volumes of DDW (0, 10, 20, 50, 60, and 70 mL) were then added to 10 mL of diluted  $\text{CaCl}_2$  followed by the addition of 10 mL of diluted  $\text{K}_2\text{CO}_3$  at different feeding rates (1, 1.5, 2, and 2.5 h). The procedure was repeated using three different solvents of reaction, namely, methanol, Analytical Reagent Grade, Lot No. 1,352,421 (Sigma Aldrich, Steinheim, Germany); 70% ethanol, ChemPur<sup>®</sup> CAS No. 64-17-5 (System, GmbH, Karlsruhe, Germany); or propanol, Analytical Reagent Grade, Lot No. 1,367,431 (Sigma Aldrich, Steinheim, Germany). The solutions were then left for 24 h to precipitate. Then, the supernatant solution was discarded and the resultant product was centrifuged using Eppendorf Centrifuge 5804 (Eppendorf North America Inc., Enfield, CT, USA) at 7000 rpm for 7 min. The acidity of the resultant solution was then neutralized by washing three times with DDW. The resultant product was either dried using a Memmert oven 100–800 (Mettler, Schwabach, Germany) at 110  $^\circ\text{C}$  for 24 h or by freeze drying; first by putting the resultant product in the Ilshin Europe Biobase DF8517 freezer (Ilshin Lab Co. Ltd., Ede, Netherlands) at  $-80$   $^\circ\text{C}$  for 3 h and then at  $-108$   $^\circ\text{C}$  for 48 h in the freeze-drying machine (Scanvac CoolSafe 4.5L, LaboGene ApS, Allerød, Denmark).

The  $\text{CaCO}_3$  powder derived from cockle shell, obtained using different parameters, was first characterized using a field-emission scanning electron microscope equipped with energy-dispersive X-ray (FESEM-EDX), LEICA EM SCD005, (Leica, Tokyo, Japan) to evaluate its morphology, particle size, and elemental composition. Then, the  $\text{CaCO}_3$  powder was characterized with the Brunauer–Emmett–Teller (BET) method using TristarII (Micromeritics Instrument Corporation, Norcross, GA, USA) for its average surface area and pore diameter. Once the optimization of  $\text{CaCO}_3$  powder was achieved, it was then characterized with an X-ray diffractometer (XRD) using a Shimadzu XRD–6000 (Shimadzu Corporation, Kyoto, Japan) to study its crystallinity and phases using  $\text{Cu K}\alpha$  radiation ( $\lambda = 1.5406$  Å, 40 kV at 30 mA). Then, the  $\text{CaCO}_3$  powder was also characterized with Fourier transform infrared (FTIR) spectroscopy using an FTIR SPECTRUM RX1 (Perkin Elmer Inc. Hopkinton, MA, USA) spectrometer in the range of 600–4000  $\text{cm}^{-1}$  for determination of the chemical bonding of chemical substances.

The thermal stability of  $\text{CaCO}_3$  was then investigated with thermogravimetric analysis (TGA), using an SSC/5200 TG/DTA 220 (Seiko Instrument, Tokyo, Japan) with a temperature range of 50–900  $^\circ\text{C}$  and scan rate of 20  $^\circ\text{C}/\text{min}$  under  $\text{N}_2$  atmosphere.

The optimized  $\text{CaCO}_3$  was then calcined at 750  $^\circ\text{C}$  for 30 min using a Standard Digital Muffles Furnace FH 27 (DAIHAN Scientific Co., Ltd., Gangwon-do, Korea) to produce  $\text{CaO}$  powder. The  $\text{CaO}$

powder was then characterized using SEM, XRD, and FTIR. Figure 1 summarizes the overall synthetic reaction to produce and convert  $\text{CaCO}_3$  to  $\text{CaO}$ . The morphology of  $\text{CaO}$  derived from cockle shell was compared to commercial  $\text{CaO}$  98%, <160 nm (Sigma Aldrich, Steinheim, Germany) using FESEM.

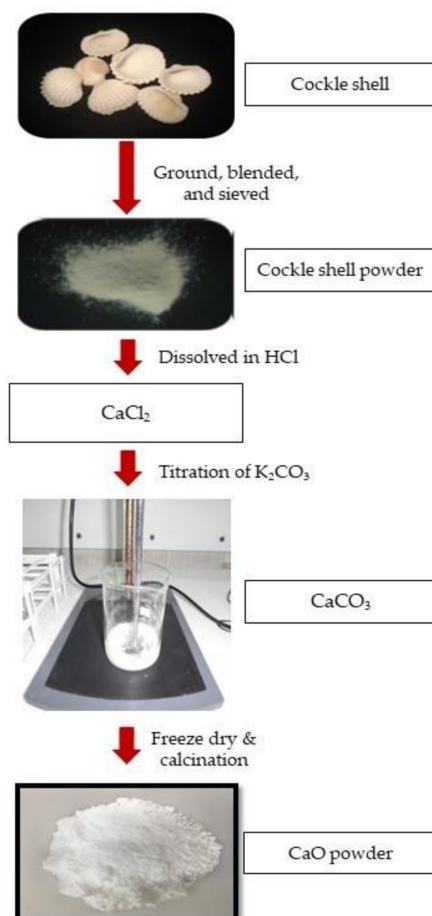


**Figure 1.** Schematic diagram of  $\text{CaCO}_3$  and  $\text{CaO}$  synthetic procedure.

### 3. Results and Discussion

#### 3.1. FESEM/EDX and BET Analyses of $\text{CaCO}_3$ Particles Using Different Parameters

Figure 2 indicates the effect of different volumes of DDW on the morphology of the  $\text{CaCO}_3$  derived from cockle shells. Samples of  $\text{CaCO}_3$  prepared by diluting  $\text{CaCl}_2$  with 50 mL of DDW, as shown in Figure 2d, exhibited spherical-like, well-dispersed crystals with even size. However, other samples of  $\text{CaCO}_3$  prepared with different DDW volumes exhibited clumped and agglomerated masses of crystals with irregular shapes and sizes. It may be explained that an increased amount of DDW resulted in greater dilution of samples, which provided more space for the movement of nanoparticles. However, as the volume of DDW increased, these molecules tended to be more solvated due to excess absorption of water, thus increasing in size and leading to agglomeration. Calcium carbonate prepared using 50 mL of DDW dilution had an average particle size of 39 nm, which was smaller in comparison to other samples. BET surface area analysis also revealed that using 50 mL of DDW gave the largest surface area and the smallest pore diameter of  $\text{CaCO}_3$  in comparison to other samples, as shown in Table 1. The smaller particle size is related to a larger surface area and smaller pore diameter.  $\text{CaCO}_3$ , with various morphologies, have been fabricated previously. This has included cubic and needle shaped particles [36] where polyacrylamide was used, and rod-shaped particles [6] where a microemulsion system was used.

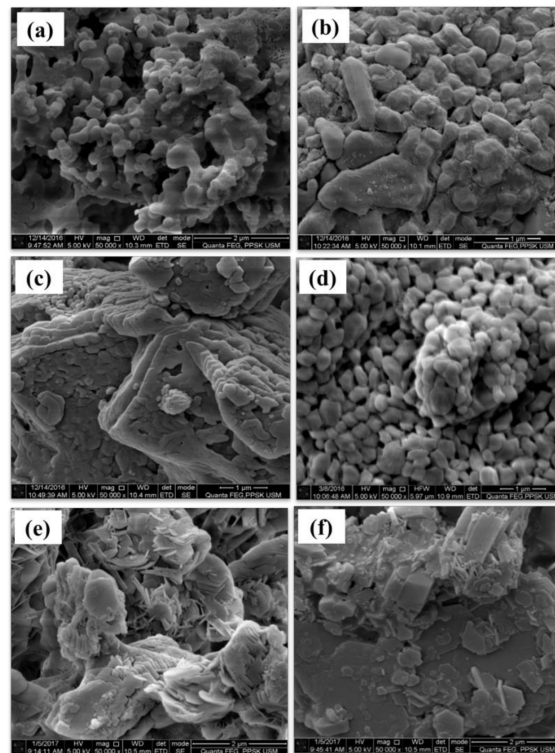


**Figure 2.** FESEM images of  $\text{CaCO}_3$  at different volumes of distilled water: (a) 0 mL; (b) 10 mL; (c) 20 mL; (d) 50 mL; (e) 60 mL; and (f) 70 mL.

**Table 1.** Brunauer–Emmett–Teller (BET) average surface area, pore diameter of  $\text{CaCO}_3$  in different volumes of double-distilled water (DDW).

Volume of DDW (mL)	Surface Area ( $\text{m}^2/\text{g}$ )	Average Pore Diameter ( $\text{Å}$ )
0	8.53	386
10	14.9	235
20	16.8	281
50	26.0	180
60	25.0	183
70	25.8	192

The morphology of  $\text{CaCO}_3$  using the different polar solvents methanol, ethanol, and propanol is illustrated in Figure 3. The particle size and average pore diameter of  $\text{CaCO}_3$  are tabulated in Table 2, where  $\text{CaCO}_3$  particles, in all solvent systems except ethanol, possessed macroporous structure with a range of more than 50 nm, which is in accordance with Zdravkov et al. [37]. From the FESEM images, the samples prepared with ethanol displayed spherical calcite crystals, which were evenly dispersed and more symmetrical in structure when compared to methanol and propanol. The use of ethanol slowed down the chemical reaction, and hence the particles acquired a spherical shape with no agglomeration. Ethanol was used in other studies [38,39] and showed similar results with the current study. This phenomenon is probably due to the presence of smaller and more active  $-\text{OH}$  and  $-\text{C}_2\text{H}_5$  groups in ethanol, which is reported to be effective in eliminating water molecules [40] that cause more agglomeration to form larger molecules [39]. The enhancement of the particle size upon the addition of ethanol was reported to be due to the reduction of the energy of atomization as a consequence of the decrease in the vapour pressure of the solution, owing to their slow evaporation [41,42].

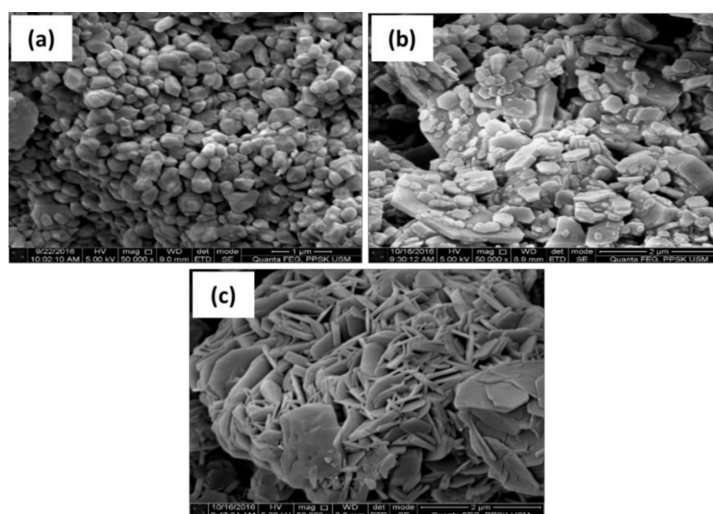


Figure 3. FESEM images of CaCO<sub>3</sub> in different solvents: (a) ethanol; (b) methanol; and (c) propanol.

Table 2. BET surface area and average pore diameter analyses of CaCO<sub>3</sub> in different organic solvents.

Solvent	Surface Area (m <sup>2</sup> /g)	Average Pore Diameter (Å)
Propanol	0.96	523
Ethanol	7.1	409
Methanol	6.3	703

The effect of the K<sub>2</sub>CO<sub>3</sub> feeding rate on the morphology of CaCO<sub>3</sub> nanoparticles in ethanolic solution is shown in Figure 4. It can be seen that the 1 h feeding rate of K<sub>2</sub>CO<sub>3</sub> had led to the formation of spherical CaCO<sub>3</sub> with clear surface and high sphericity. However, as the feeding rate was increased, the shape of the particles was distorted and their form changed with more agglomeration of the particles. The surface area and average pore diameter of CaCO<sub>3</sub> are tabulated in Table 3. As the feeding rate increased, the surface area decreased and pore diameter increased, which is similar to a previous study by Chen et al. [43] where hollow microspheres increased as the feeding rate increased. This was probably attributed to the Ostwald ripening process, where larger particles begin to grow and consume the smaller particles due to the difference in concentration gradient [44].

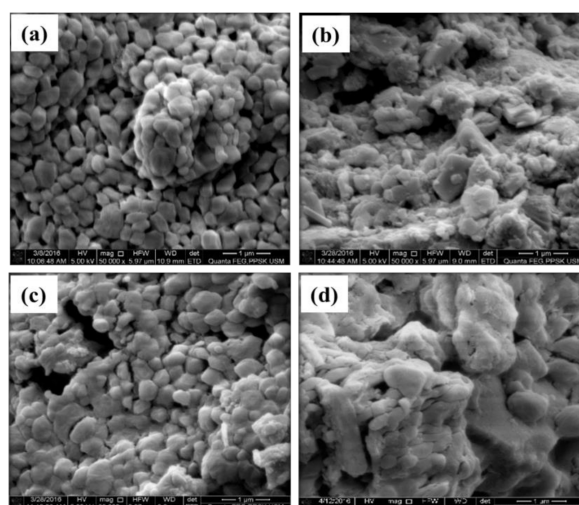
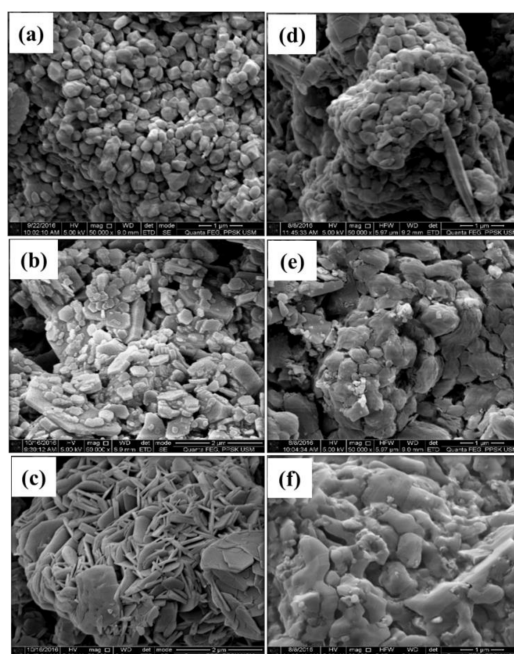


Figure 4. FESEM images of CaCO<sub>3</sub> using differing feeding rates of K<sub>2</sub>CO<sub>3</sub>: (a) 1 h; (b) 1.5 h; (c) 2 h; and (d) 2.5 h.

**Table 3.** BET surface area and average pore diameter analyses of CaCO<sub>3</sub> at different feeding rates of K<sub>2</sub>CO<sub>3</sub>.

Feeding Rate of K <sub>2</sub> CO <sub>3</sub> (h)	Surface Area (m <sup>2</sup> /g)	Average Pore Diameter (Å)
1.0	26	580
1.5	8.4	606
2.0	5.9	758
2.5	4.1	325

The effect of different drying methods on the morphology of CaCO<sub>3</sub> nanoparticles is shown in Figure 5. The CaCO<sub>3</sub> nanoparticles prepared in the ethanolic solution and then freeze-dried exhibited structurally well-organized, more uniform spherical shapes with less agglomeration compared to the oven-drying technique. This is probably because oven drying may produce uneven and overheating of the material, where the material does not have sufficient time to take its proper shape, leading to agglomeration of the particles. These current results are supported by another study [45].

**Figure 5.** FESEM images of CaCO<sub>3</sub> prepared in (a,d) ethanol; (b,e) methanol; and (c,f) propanol after freeze drying (left) and oven drying (right).

### 3.2. XRD Analysis of Optimized CaCO<sub>3</sub> Nanoparticles

Based on the aforementioned parameters, the optimal conditions for the formation of spherical nanoparticles of CaCO<sub>3</sub> were 50 mL of DDW with 1 h feeding rate of K<sub>2</sub>CO<sub>3</sub> in ethanolic solution, using the freeze-drying technique. Figure 6 shows the XRD analysis of the composition and phase of the optimized CaCO<sub>3</sub> nanoparticles derived from cockle shell. The presence of CaCO<sub>3</sub> can be observed at 2θ of 23.0, 29.5, 36.0, 39.3, 43.2, 48.5, 57.5, 60.9, 63.1, 64.4, 65.6, and 83.7°. These 2θ positions correspond to (0 1 2), (1 0 4), (1 1 0), (1 1 3), (2 0 2), (1 1 6), (1 2 2), (2 1 4), (1 2 5), (0 3 0), (0 0 12), and (1 3 4) crystal planes, respectively. Other parameters such as a = b = 4.9900 Å, c = 17.0020 Å, α = β = 90.0000°, and γ = 120.0000° were also obtained. The assignments of 2θ position and other parameters for CaCO<sub>3</sub> from XRD were in agreement with the reference code 98-000-5340 of a hexagonal crystal system and space group R-3c. The crystallite size of CaCO<sub>3</sub> nanoparticles was 61.4 nm, which was calculated from the Debye–Scherrer equation,  $L = K\lambda/\beta \cos 2\theta$ , where K is a constant; λ is to the X-ray wavelength (λ = 1.54060 Å), β is the full-width at half maximum, and θ is the angle. The formation of the calcite

phase of  $\text{CaCO}_3$  in the current investigation matched well with the results of Kontoyonis et al. [46], with the characteristic peak positioned at  $2\theta = 29.5^\circ$  and the crystal plane of (1 0 4).

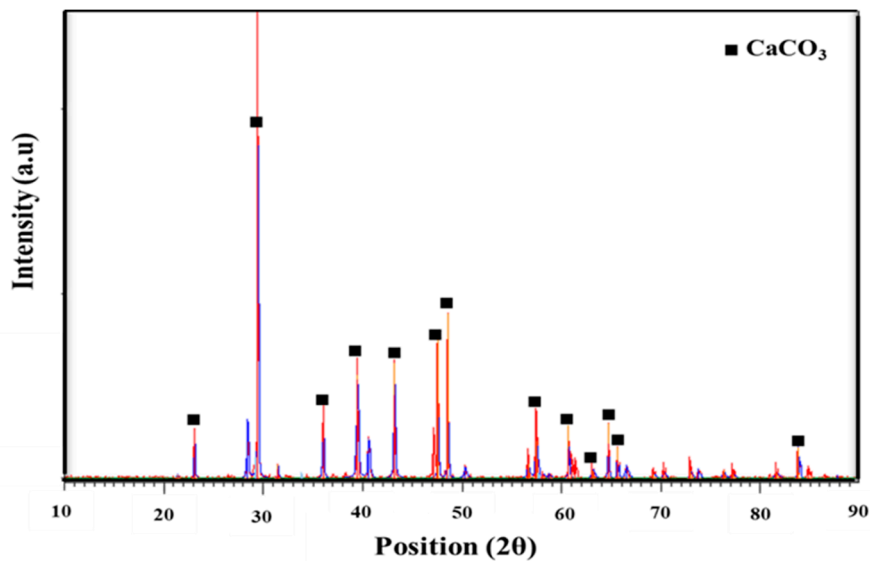


Figure 6. XRD analysis of  $\text{CaCO}_3$ .

### 3.3. EDX Analysis of Optimized $\text{CaCO}_3$ Nanoparticles

The elemental composition of the optimized  $\text{CaCO}_3$  nanoparticles is shown in Figure 7. The expected elements such as Ca, C, and O were present in the  $\text{CaCO}_3$  derived from cockle shells, indicating the success of the sol-gel method.

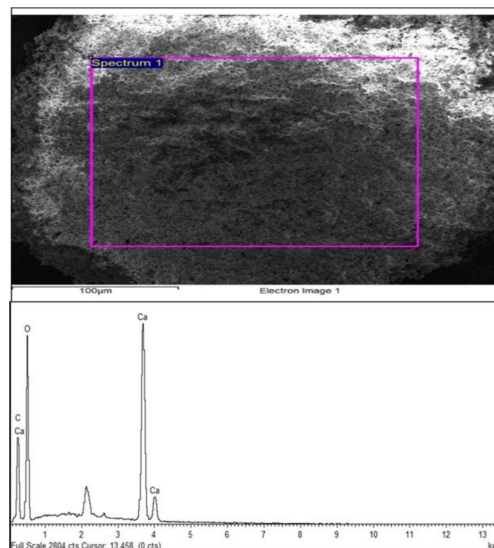


Figure 7. EDX spectrum of  $\text{CaCO}_3$  nanoparticles.

### 3.4. FTIR Analysis of Optimized $\text{CaCO}_3$ Nanoparticles

The FTIR of  $\text{CaCO}_3$  is shown in Figure 8. According to Wang et al. [47], due to the different vibration modes of  $\text{CO}_3^{2-}$ , four normal vibration modes of  $\text{CO}_3^{2-}$  can be obtained, namely, doubly degenerate planar bending, symmetric stretching, out-of-plane bending, and in-plane bending, which appeared at  $1420\text{ cm}^{-1}$ ,  $1093\text{ cm}^{-1}$ ,  $880\text{ cm}^{-1}$ , with a very weak vibration mode at around  $700\text{ cm}^{-1}$

respectively, which confirms the formation of  $\text{CaCO}_3$  [48]. The peak at  $3644\text{ cm}^{-1}$  is due to the O-H bond from the adsorbed water molecule.

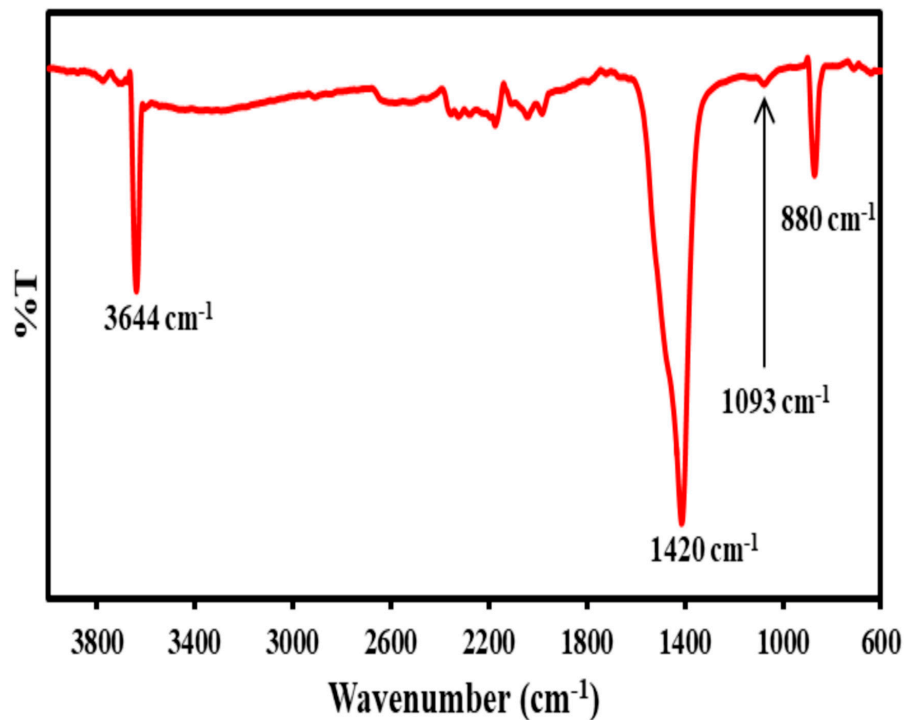


Figure 8. FTIR spectrum of  $\text{CaCO}_3$ .

### 3.5. TGA of Optimized $\text{CaCO}_3$ Nanoparticles

Figure 9 illustrates the TGA of  $\text{CaCO}_3$ , where the first weight loss of around 22% was due to water loss, which occurred at around  $100\text{ }^\circ\text{C}$ . The second weight loss of around 25% was due to the decomposition of  $\text{CaCO}_3$  to  $\text{CaO}$  and  $\text{CO}_2$  [49], which started from around  $500\text{--}700\text{ }^\circ\text{C}$ . This is in agreement with Popescu et al. [50], who reported the formation of calcite  $\text{CaCO}_3$  at  $459\text{ }^\circ\text{C}$ . The  $\text{CaO}$  was expected to completely form after  $700\text{ }^\circ\text{C}$  [49]. The purity of the  $\text{CaO}$  detected by TGA curves was 53.30% while the purity of  $\text{CaO}$  was  $56\% \pm 3\%$ , which is considered standard of pure  $\text{CaO}$ .

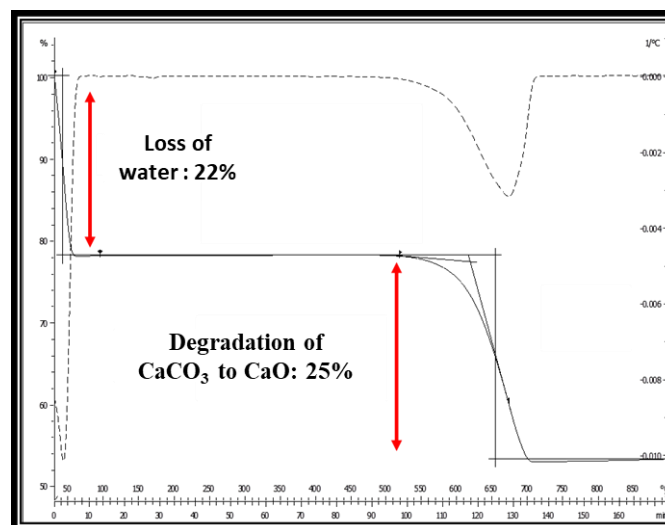
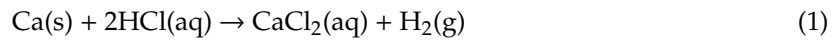


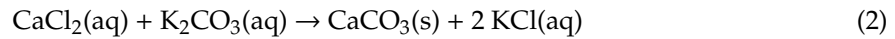
Figure 9. TGA of  $\text{CaCO}_3$ .

Therefore, based on the TGA results it can be suggested that the formation of CaO involved a few steps of chemical reactions, namely, dissolution reaction, precipitation reaction, and degradation reaction, as depicted in Equations (1)–(3) below.

Dissolution reaction:



Precipitation reaction:



Degradation reaction:



### 3.6. FTIR Analysis of CaO Nanoparticles

From Figure 10, the formation of CaO can be observed at  $721\text{ cm}^{-1}$ , which can be assigned as Ca-O bond, as previously reported by Rudy Syah Putra et al. [51]. Furthermore, the presence of CaO after the calcination of  $\text{CaCO}_3$  can be further observed at  $1420\text{ cm}^{-1}$  and  $875\text{ cm}^{-1}$ , which is in agreement with Guan et al. [52].

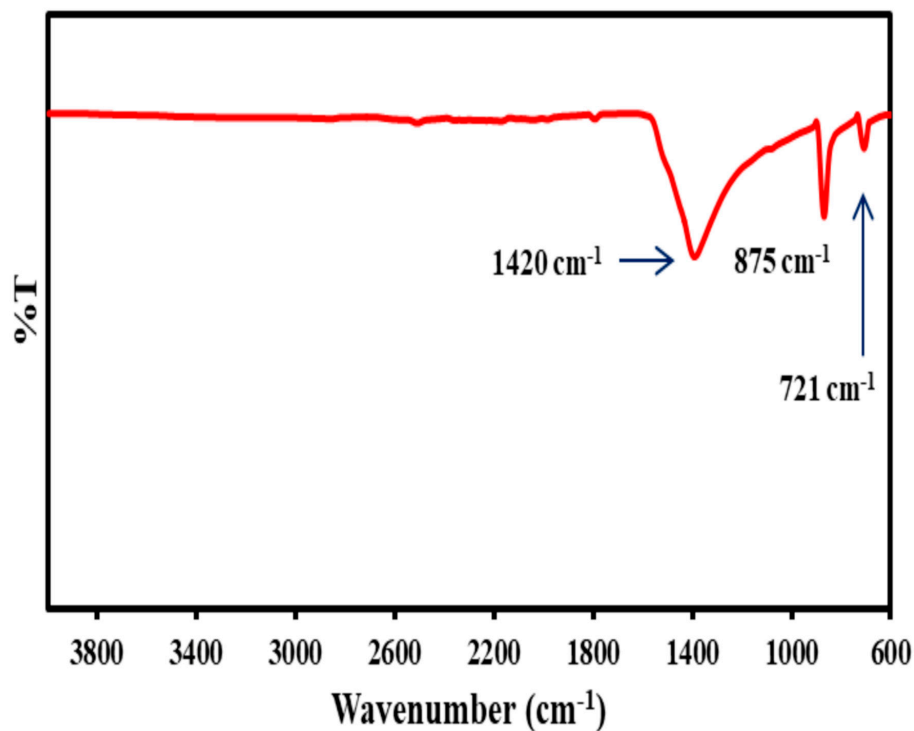


Figure 10. FTIR spectrum of CaO.

### 3.7. XRD Analysis of CaO Nanoparticles

Figure 11 shows the XRD analysis of CaO powder derived from cockle shells. The high and narrow intense peaks depict the structural crystallization of the CaO. The formation of CaO can be observed at  $2\theta = 29, 36, 39, 47,$  and  $48^\circ$ , which is accordance with Bai et al. [53] who prepared CaO from 0.3 M sodium carbonate ( $\text{Na}_2\text{CO}_3$ ) and 0.3 M calcium chloride ( $\text{CaCl}_2$ ). Therefore, the formation of the CaO derived from cockle shell can be successfully synthesized by the sol–gel method.

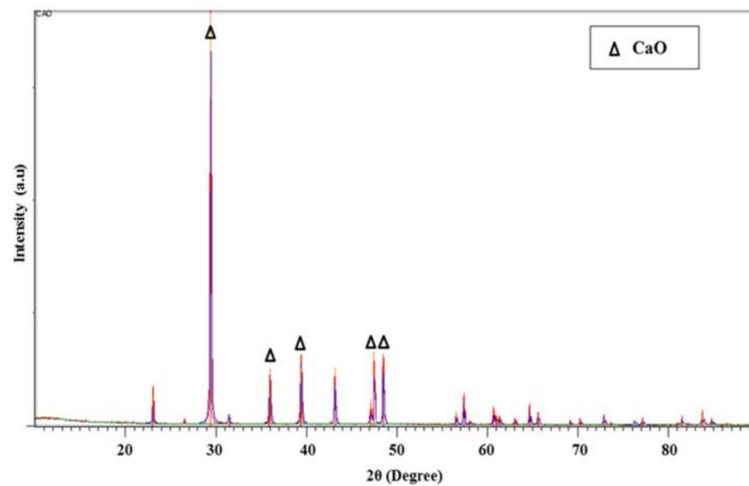


Figure 11. XRD analysis of CaO.

### 3.8. FESEM Analysis of CaO Nanoparticles

Figure 12a,b illustrate the FESEM images of CaO derived from cockle shells and commercially obtained CaO respectively. The magnified images of both cockle-shell-derived CaO and commercial CaO show that they were evenly dispersed and structurally similar. The average particle sizes of CaO derived from cockle shells and commercially obtained CaO were 22–70 nm and 32–159 nm, respectively. The CaO obtained in the current study was used to stabilize zirconia, which showed good properties as a potential dental material [9].

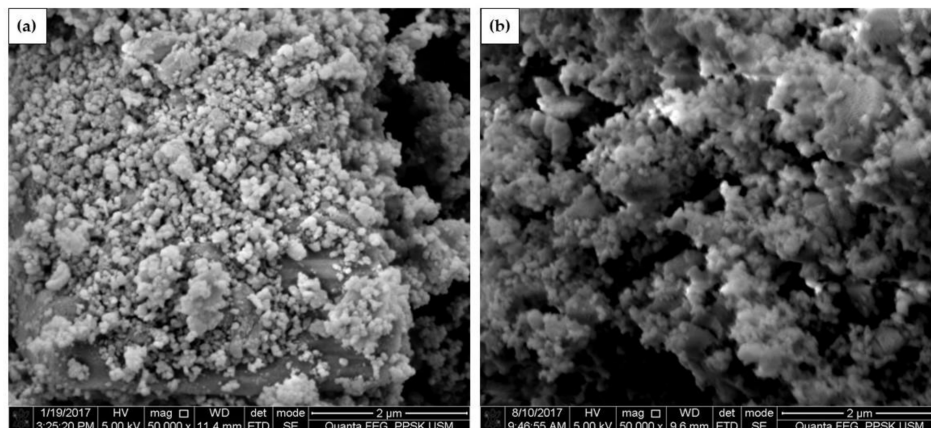


Figure 12. FESEM images of CaO: (a) derived from cockle shell; (b) commercial.

## 4. Conclusions

Well-structured spherical  $\text{CaCO}_3$  of calcite phase was obtained from the optimum conditions by adding 50 mL DDW into  $\text{CaCl}_2$  in ethanolic solution with a feeding rate of  $\text{K}_2\text{CO}_3$  of 1 h using the freeze-drying method. Less agglomeration was obtained by the freeze-drying technique with the surface area of  $26 \text{ m}^2/\text{g}$  and average particle size of 39 nm. Spherical nanosized CaO (22–70 nm) was obtained when the  $\text{CaCO}_3$  was calcined at  $750 \text{ }^\circ\text{C}$  for 30 min.

**Author Contributions:** Conceptualization, Z.A.-G., A.I.H., I.A.R., A.H.; methodology, A.I.H., I.A.R., A.N.C.M., N.A.A.G.; software, A.I.H., A.N.C.M., N.A.A.G.; validation, Z.A.-G., I.A.R., A.H.; formal analysis, A.I.H., A.N.C.M., N.A.A.G.; investigation, A.I.H., A.N.C.M.; resources, Z.A.-G., I.A.R., A.H.; data curation, A.I.H., A.N.C.M., N.A.A.G.; writing—original draft preparation, A.I.H., Z.A.-G., A.N.C.M.; writing—review and editing, Z.A.-G., A.H., I.A.R.; supervision, Z.A.-G., I.A.R., A.H.; project administration, Z.A.-G.; funding acquisition, Z.A.-G., I.A.R., A.H. All authors have read and agreed to the published version of the manuscript.

**Funding:** This research was funded by Science Fund from the Ministry of Science, Technology and Innovation (MOSTI) with the grant number: 07-01-05 SF0845 (305/PPSG/6113701).

**Acknowledgments:** The authors would like to acknowledge all Multidisciplinary Laboratory administrative and technical staff for their kind support throughout the research work.

**Conflicts of Interest:** The authors declare no conflict of interest.

## References

1. Jaji, A.Z.; Zuki, A.; Mahmud, R.; Loqman, M.Y.; Hezmee, M.N.M.; Isa, T.; Wenliang, F.; Hammadi, N.I. Synthesis, characterization, and cytocompatibility of potential cockle shell aragonite nanocrystals for osteoporosis therapy and hormonal delivery. *Nanotechnol. Sci. Appl.* **2017**, *10*, 23–33. [[CrossRef](#)]
2. Maleki, S.; Barzegar-Jalali, M.; Zarrintan, M.H.; Adibkia, K.; Lotfipour, F. Calcium carbonate nanoparticles; potential applications in bone and tooth disorders. *Pharm. Sci.* **2015**, *20*, 175–182.
3. Kharissova, O.V.; Dias, H.R.; Kharisov, B.I.; Pérez, B.O.; Pérez, V.M.J. The greener synthesis of nanoparticles. *Trends Biotechnol.* **2013**, *31*, 240–248. [[CrossRef](#)]
4. Awang-Hazmi, A.; Zuki, A.; Noordin, M.; Jalila, A.; Norimah, Y. Mineral Composition of the Cockle (*Anadara granosa*) Shells of West Coast of Peninsular Malaysia and It's Potential as Biomaterial for Use in Bone Repair. *J. Anim. Vet. Adv.* **2007**, *6*, 591–594.
5. Ghafar, S.L.M.A.; Hussein, M.Z.; Rukayadi, Y.; Zakaria, Z.A.B. Surface-functionalized cockle shell-based calcium carbonate aragonite polymorph as a drug nanocarrier. *Nanotechnol. Sci. Appl.* **2017**, *10*, 79–94. [[CrossRef](#)]
6. Kamba, A.S.; Ismail, M.; Ibrahim, T.A.T.; Zuki, A. Synthesis and Characterisation of Calcium Carbonate Aragonite Nanocrystals from Cockle Shell Powder (*Anadara granosa*). *J. Nanomater.* **2013**, *2013*, 1–9. [[CrossRef](#)]
7. Mahmood, S.; Zuki, A.; Razak, I.S.A.; Yusof, L.M.; Jaji, A.Z.; Tijani, I.; Hammadi, N.I. Preparation and characterization of cockle shell aragonite nanocomposite porous 3D scaffolds for bone repair. *Biochem. Biophys. Rep.* **2017**, *10*, 237–251. [[CrossRef](#)]
8. Mailafiya, M.M.; Abubakar, K.; Danmaigoro, A.; Chiroma, S.M.; Rahim, E.B.A.; Moklas, M.A.M.; Zuki, A. Cockle Shell-Derived Calcium Carbonate (Aragonite) Nanoparticles: A Dynamite to Nanomedicine. *Appl. Sci.* **2019**, *9*, 2897. [[CrossRef](#)]
9. Hussein, A.I.; Mat, A.N.C.; Wahab, N.A.A.A.; Ab Rahman, I.; Husein, A.; Ab-Ghani, Z. Synthesis and Properties of Novel Calcia-Stabilized Zirconia (Ca-SZ) with Nano Calcium Oxide Derived from Cockle Shells and Commercial Source for Dental Application. *Appl. Sci.* **2020**, *10*, 5751. [[CrossRef](#)]
10. Vinas, M.T.; Zhang, F.; Vleugels, J.; Anglada, M. Effect of calcia co-doping on ceria-stabilized zirconia. *J. Eur. Ceram. Soc.* **2018**, *38*, 2621–2631. [[CrossRef](#)]
11. Papanagiotou, H.P.; Morgano, S.M.; Giordano, R.A.; Pober, R. In vitro evaluation of low-temperature aging effects and finishing procedures on the flexural strength and structural stability of Y-TZP dental ceramics. *J. Prosthet. Dent.* **2006**, *96*, 154–164. [[CrossRef](#)]
12. Beyth, N.; Houri-Haddad, Y.; Domb, A.J.; Khan, W.; Hazan, R. Alternative Antimicrobial Approach: Nano-Antimicrobial Materials. *Evid. Based Complement. Altern. Med.* **2015**, *2015*, 1–16. [[CrossRef](#)]
13. Grochowska, K.; Siuzdak, K.; Karczewski, J.; Śliwiński, G. Functionalization of indium-tin-oxide electrodes by laser-nanostructured gold thin films for biosensing applications. *Appl. Surf. Sci.* **2015**, *357*, 1684–1691. [[CrossRef](#)]
14. Espinosa, K.R.; Castillo, L.A.; Barbosa, S.E. Blown nanocomposite films from polypropylene and talc. Influence of talc nanoparticles on biaxial properties. *Mater. Des.* **2016**, *111*, 25–35. [[CrossRef](#)]
15. Abt, T.; Sánchez-Soto, M. A Review of the Recent Advances in Cyclic Butylene Terephthalate Technology and its Composites. *Crit. Rev. Solid State Mater. Sci.* **2016**, *42*, 173–217. [[CrossRef](#)]
16. Lu, J.; Lu, Z.; Li, X.; Xu, H.; Li, X. Recycling of shell wastes into nanosized calcium carbonate powders with different phase compositions. *J. Clean. Prod.* **2015**, *92*, 223–229. [[CrossRef](#)]
17. Kurokawa, H. Temporal change of polished surface of composite resin. *Jpn. J. Conserv. Dent.* **2007**, *50*, 17.
18. Afrashtehfar, K.I.; Del Fabbro, M. Clinical performance of zirconia implants: A meta-review. *J. Prosthet. Dent.* **2020**, *123*, 419–426. [[CrossRef](#)]

19. Raigrodski, A.J. Contemporary materials and technologies for all-ceramic fixed partial dentures: A review of the literature. *J. Prosthet. Dent.* **2004**, *92*, 557–562. [[CrossRef](#)]
20. Dion, I.; Rouais, F.; Baquey, C.; Lahaye, M.; Salmon, R.; Trut, L.; Cazorla, J.P.; Huong, P.V.; Monties, J.R.; Havlik, P. Physico-chemistry and cytotoxicity of ceramics: Part I—Characterization of ceramic powders. *J. Mater. Sci. Mater. Electron.* **1997**, *8*, 325–332. [[CrossRef](#)]
21. Nakonieczny, D.; Paszenda, Z.; Drewniak, S.; Radko, T.; Lis, M. sZrO<sub>2</sub>-CeO<sub>2</sub> ceramic powders obtained from a sol-gel process using acetylacetone as a chelating agent for potential application in prosthetic dentistry. *Acta Bioeng. Biomech.* **2016**, *18*, 53–60.
22. Nakonieczny, D.; Walke, W.; Majewska, J.; Paszenda, Z. Characterization of magnesia-doped yttria-stabilized zirconia powders for dental technology applications. *Acta Bioeng. Biomech.* **2014**, *16*, 16.
23. Piconi, C.; Maccauro, G. Zirconia as a ceramic biomaterial. *Biomaterials* **1999**, *20*, 1–25. [[CrossRef](#)]
24. Tanaka, K.; Tamura, J.; Kawanabe, K.; Nawa, M.; Oka, M.; Uchida, M.; Kokubo, T.; Nakamura, T. Ce-TZP/Al<sub>2</sub>O<sub>3</sub> nanocomposite as a bearing material in total joint replacement. *J. Biomed. Mater. Res.* **2002**, *63*, 262–270. [[CrossRef](#)]
25. Christel, P.; Meunier, A.; Heller, M.; Torre, J.P.; Peille, C.N. Mechanical properties and short-term in vivo evaluation of yttrium-oxide-partially-stabilized zirconia. *J. Biomed. Mater. Res.* **1989**, *23*, 45–61. [[CrossRef](#)]
26. Hannink, R.H.J.; Kelly, P.M.; Muddle, B.C. Transformation Toughening in Zirconia-Containing Ceramics. *J. Am. Ceram. Soc.* **2004**, *83*, 461–487. [[CrossRef](#)]
27. Nath, S.; Sinha, N.; Basu, B. Microstructure, mechanical and tribological properties of microwave sintered calcia-doped zirconia for biomedical applications. *Ceram. Int.* **2008**, *34*, 1509–1520. [[CrossRef](#)]
28. Gempita, G.; Hasratiningsih, Z.; Subrata, G.; Purwasasmita, B.S. Synthesis of mesh-shaped calcia partially stabilized zirconia using eggshell membrane template as filler composite. *Padjadjaran J. Dent.* **2017**, *29*, 29. [[CrossRef](#)]
29. Papahadjopoulos-Sternberg, B.; Ackrell, J. Seeing Multifunctional Nano- and Micro-particles Suitable for Imaging & Therapy Using Freeze-fracture Electron Microscopy. *Microsc. Microanal.* **2008**, *14*, 1604–1605. [[CrossRef](#)]
30. 3Kumar, A.; Yadav, N.; Bhatt, M.; Mishra, N.K.; Chaudhary, P.; Singh, R. Sol-gel derived nanomaterials and its applications: A review. *Res. J. Chem. Sci.* **2015**, *5*, 98–105.
31. De Choudens-Sanchez, V.; Gonzalez, L.A. Calcite and Aragonite Precipitation Under Controlled Instantaneous Supersaturation: Elucidating the Role of CaCO<sub>3</sub> Saturation State and Mg/Ca Ratio on Calcium Carbonate Polymorphism. *J. Sediment. Res.* **2009**, *79*, 363–376. [[CrossRef](#)]
32. Góna, K.; Hund, M.; Vučak, M.; Gröhn, F.; Wegner, G. Amorphous calcium carbonate in form of spherical nanosized particles and its application as fillers for polymers. *Mater. Sci. Eng. A* **2008**, *477*, 217–225. [[CrossRef](#)]
33. Buasri, A.; Chaiyut, N.; Loryuenyong, V.; Worawanitchaphong, P.; Trongyong, S. Calcium Oxide Derived from Waste Shells of Mussel, Cockle, and Scallop as the Heterogeneous Catalyst for Biodiesel Production. *Sci. World J.* **2013**, *2013*, 1–7. [[CrossRef](#)]
34. Ghazali, S.S.; Kem, K.L.; Jusoh, R.; Abdullah, S.; Shariffuddin, J.H. Evaluation of La-Doped CaO Derived from Cockle Shells for Photodegradation of POME. *Bull. Chem. React. Eng. Catal.* **2019**, *14*, 205–218. [[CrossRef](#)]
35. Laonapakul, T.; Sutthi, R.; Chaikool, P.; Mutoh, Y.; Chindaprasitrd, P. Optimum conditions for preparation of bio-calcium from blood cockle and golden apple snail shells and characterization. *Sci.* **2019**, *45*, 10–20. [[CrossRef](#)]
36. Wang, C.; Zhao, J.; Zhao, X.; Bala, H.; Wang, Z. Synthesis of nanosized calcium carbonate (aragonite) via a polyacrylamide inducing process. *Powder Technol.* **2006**, *163*, 134–138. [[CrossRef](#)]
37. Zdravkov, B.D.; Čermák, J.J.; Šefara, M.; Janků, J. Pore classification in the characterization of porous materials: A perspective. *Open Chem.* **2007**, *5*, 385–395. [[CrossRef](#)]
38. Khodae, P.; Najmoddin, N.; Shahrada, S. The effect of ethanol and temperature on the structural properties of mesoporous silica synthesized by the sol-gel method. In Proceedings of the 2018 25th National and 3rd International Iranian Conference on Biomedical Engineering (ICBME), Qom, Iran, 29–30 November 2018; pp. 1–5.
39. Bahar, M.; Mozaffari, M.; Esmaili, S. Effect of different alcohols, gelatinizing times, calcination and microwave on characteristics of TiO<sub>2</sub> nanoparticles synthesized by sol-gel method. *J. Theor. Appl. Phys.* **2017**, *11*, 79–86. [[CrossRef](#)]

40. Zhu, Y.; Zhang, L.; Gao, C.; Cao, L. The synthesis of nanosized TiO<sub>2</sub> powder using a sol-gel method with TiCl<sub>4</sub> as a precursor. *J. Mater. Sci.* **2000**, *35*, 4049–4054. [[CrossRef](#)]
41. Stein, S.W.; Myrdal, P.B. The Relative Influence of Atomization and Evaporation on Metered Dose Inhaler Drug Delivery Efficiency. *Aerosol Sci. Technol.* **2006**, *40*, 335–347. [[CrossRef](#)]
42. Smyth, H.D. Multimodal particle size distributions emitted from HFA-134a solution pressurized metered-dose inhalers. *AAPS PharmSciTech* **2003**, *4*, 76–86. [[CrossRef](#)]
43. Chen, P.; Ye, N.; He, C.; Tang, L.; Li, S.; Sun, L.; Lia, Y. Preparation of Polyacrylate Hollow Microspheres via Facile Spray Drying. *Appl. Sci.* **2019**, *9*, 228. [[CrossRef](#)]
44. Kumar, V.; Singh, K.; Kumar, A.; Kumara, M.; Singh, K.; Vij, A.; Thakur, A. Effect of solvent on crystallographic, morphological and optical properties of SnO<sub>2</sub> nanoparticles. *Mater. Res. Bull.* **2017**, *85*, 202–208. [[CrossRef](#)]
45. Krokida, M.K.; Maroulis, Z.B. Effect of drying method on shrinkage and porosity. *Dry. Technol.* **1997**, *15*, 2441–2458. [[CrossRef](#)]
46. Kontoyannis, C.G.; Vagenas, N.V. Calcium carbonate phase analysis using XRD and FT-Raman spectroscopy. *Analyst* **2000**, *125*, 251–255. [[CrossRef](#)]
47. Wang, Y.; Moo, Y.X.; Chen, C.; Gunawan, P.; Xu, R. Fast precipitation of uniform CaCO<sub>3</sub> nanospheres and their transformation to hollow hydroxyapatite nanospheres. *J. Colloid Interface Sci.* **2010**, *352*, 393–400. [[CrossRef](#)]
48. Alba-Rubio, A.C.; Santamaría-González, J.; Mérida-Robles, J.M.; Moreno-Tost, R.; Martín-Alonso, D.; Jiménez-López, A.; Maireles-Torres, P. Heterogeneous transesterification processes by using CaO supported on zinc oxide as basic catalysts. *Catal. Today* **2010**, *149*, 281–287. [[CrossRef](#)]
49. Karunadasa, K.S.; Manoratne, C.; Pitawala, H.; Rajapakse, R. Thermal decomposition of calcium carbonate (calcite polymorph) as examined by in-situ high-temperature X-ray powder diffraction. *J. Phys. Chem. Solids* **2019**, *134*, 21–28. [[CrossRef](#)]
50. Popescu, M.-A.; Isopescu, R.; Matei, C.; Fagarasan, G.; Plesu, V. Thermal decomposition of calcium carbonate polymorphs precipitated in the presence of ammonia and alkylamines. *Adv. Powder Technol.* **2014**, *25*, 500–507. [[CrossRef](#)]
51. Putra, R.S.; Liyanita, A.; Arifah, N.; Puspitasari, E.; Sawaludin; Hizam, M.N. Enhanced Electro-Catalytic Process on the Synthesis of FAME Using CaO from Eggshell. *Energy Procedia* **2017**, *105*, 289–296. [[CrossRef](#)]
52. Guan, W.; Ji, F.; Cheng, Y.; Fang, Z.; Fang, D.; Yan, P.; Chen, Q. A Novel Synthesis Method of Porous Calcium Silicate Hydrate Based on the Calcium Oxide/Polyethylene Glycol Composites. *J. Nanomater.* **2013**, *2013*, 1–7. [[CrossRef](#)]
53. Bai, H.-X.; Shen, X.-Z.; Liu, X.-H.; Liu, S.-Y. Synthesis of porous CaO microsphere and its application in catalyzing transesterification reaction for biodiesel. *Trans. Nonferrous Met. Soc. China* **2009**, *19*, s674–s677. [[CrossRef](#)]

**Publisher’s Note:** MDPI stays neutral with regard to jurisdictional claims in published maps and institutional affiliations.



© 2020 by the authors. Licensee MDPI, Basel, Switzerland. This article is an open access article distributed under the terms and conditions of the Creative Commons Attribution (CC BY) license (<http://creativecommons.org/licenses/by/4.0/>).